

Nanoparticle Effects on Structure and Properties of Polypropylene Meltblown Webs

Raghavendra R. Hegde, Gajanan S. Bhat

Department of Materials Science and Engineering, The University of Tennessee, Knoxville, 37996-2200 Tennessee, USA

Received 6 March 2009; accepted 4 July 2009

DOI 10.1002/app.31089

Published online 15 September 2009 in Wiley InterScience (www.interscience.wiley.com).

ABSTRACT: The effect of nanoclay additive on the structure, morphology, and mechanical properties of polypropylene meltblown webs is reported here for the first time. Effect of nanoclay on the meltblown processing, resultant fiber web structure, and properties are discussed. Combination of wide-angle x-ray diffraction, differential scanning calorimetry, and transmission electron microscopy were used to determine the nature of clay dispersion in the polypropylene fiber matrix and resultant morphology. Transmission electron microscopy micrographs

revealed nanolevel dispersion of the additive in the fiber web. Clay additive did not offer any benefit as far as the mechanical properties of the meltblown web are concerned. Meltblown web samples with nanoclay had higher variability in web structure, high air permeability, high stiffness, and lower mechanical properties. © 2009 Wiley Periodicals, Inc. *J Appl Polym Sci* 115: 1062–1072, 2010

Key words: additives; morphology; nanocomposites; poly(propylene); structure–property relations

INTRODUCTION

Meltblowing (MB) is a one-step process in which high-velocity hot air blows a molten thermoplastic resin from an extruder die tip onto a conveyor or take-up screen to form a fine fibrous and self-bonding web. MB webs have fiber diameters generally in the range of 2 to 4 μm . MB webs produced from different polymer systems are extensively used in a wide range of applications such as filtration media, medical fabrics, adsorbent media, and sanitary products, to name only a few.^{1,2} One of the disadvantages of meltblown webs is its lack of mechanical strength. For most of the applications, it is used along with a supporting material in the composite form.

In recent years, layered silicate nanocomposites have gained enormous academic and industrial research interest.³ Continual studies have shown enhanced properties in final products derived by loading clay just as low as 0.5 wt % compared with conventional composites with large amount of micron size additives. The nanoclay dispersion is being used currently instead of conventional fillers, such as metal, glass, and wood particles, to improve modulus and tensile strength, barrier properties, flame resistance, thermal, and structural properties of many plastics.^{4–8}

Nanoclay based on montmorillonite is a layered mineral deposit of smectite family extracted from volcanic ash deposits in brine seas. Individual clay particle has high aspect ratio with surface area of around 200–600 nanometers and thickness of only 1 to few nanometers. It is known that good dispersion of clay platelets in matrix, which is also known as exfoliated morphology, gives better mechanical properties.^{6,9–15}

Influence of clay loading on properties of polypropylene (PP)–clay nanocomposites has also been studied by Liu and Wu,¹⁶ where they observed an increase in tensile strength and modulus with increase in clay content from 0 to 5 wt %. They reported increase in storage modulus, decrease in $\tan(\delta)$ and $T(g)$, and that the presence of clay additive facilitated crystallization without changing the crystal structure.

In the presence of nanoclay additive, crystallization kinetics of matrix depend both on the clay content and the interaction between polymer chain and clay platelets. Dispersed clay particles have been found to significantly influence the crystallization and polymorphism of polyesters and polyamides.^{17–19} Two mutually opposite effects, increased crystallization by nucleating ability of the additive and growth retardation, have been observed both of which are related to the content and dispersion of clay.²⁰ In principle, crystallization occurs in two stages, primary crystallization initiated by nucleation and the secondary crystallization that involves growth of spherulites until they impinge on each other. Secondary crystallization can involve thickening of the crystals or growth of new lamellae within or between existing lamellae stacks

Correspondence to: G. S. Bhat (gbhat@utk.edu).

Contract grant sponsor: Techmer PM and the Center for Materials Processing (CMP).

from remaining amorphous regions within the spherulites.^{21,22} Influence of nanoclay on the nucleation and crystallization kinetics of nylon 6, PP, and poly(ethylene terephthalate (PET) has been reported earlier.^{15,23–26}

There is continuing effort to take advantage of recent advances in nanotechnology in the textile industry. Nanoclay is one of the most affordable material that has shown promising results in polymers. Few attempts have been made to produce and study the structure and morphology of nanoclay-filled PP, nylon 6, and PET fibers.^{27–29} In melt spinning, PP with higher than 1 wt % nanoclay additive imposed processing difficulties, filament breakage, clogging in filter, and increase in melt pressure.³⁰ Effect of processing conditions on the development of morphology in nanoclay reinforced melt spun nylon 6 fibers has been carefully investigated by Ergungor et al.²⁷ Presence of nanoclay imparted substantial polymer chain orientation at moderate take up speeds because of increase in spin line stress. Also, nanoclay additive is known to promote γ -crystalline forms because of entrapment of polymer chains between platelets. In earlier studies, satisfactory color fastness has been reported for the fibers with nanoclay additive compared with neat PP.^{31,32} Also, in the presence of nanoclay, increase in moisture absorption because of increase in surface roughness, voids, and defects has been reported.²⁸ At the same draw ratio, fiber with clay had higher crystallinity and lower orientation.²⁸

Fiber formation during commercial MB process and influence of processing conditions, die to collector distance, primary air-flow rate, die temperature, and resin through put rate on the web properties have been studied earlier.^{33,34} To date, influence of nanoadditive on structure and properties of meltblown webs is not reported. In our previous studies of nanoclay on spunbond nonwovens, nucleating ability and role of clay in crystallization and spun fiber morphology were investigated.³⁵ In this study, we produced meltblown webs with very low wt % of clay additive. Influence of nanoclay, different wt % of compatibilizer, and difference in air pressure on resultant structure and properties of webs are

TABLE I
Meltblown Line Specifications

Die width	15.24 cm
Holes per die	120 holes
Die hole size	0.045 cm
Air gap	0.076 cm
Setback	0.076 cm
Throughput	0.4 g/(hole min)
Die to collector distance	38 cm
Collector speed	12 m/min
Basis weight	25.8 g/m ²

TABLE II
Sample Composition

Sample	Composition	Air pressure (kN/m ²)
Control MB	1500 MFR PP	21
1LP	0.5 % Closite Na+ and 1.25% mPP	21
1HP	0.5 % Closite Na+ and 1.25% mPP	41
2LP	0.5 % Closite Na+ and 2.5% mPP	21
2HP	0.5 % Closite Na+ and 2.5% mPP	41

studied. Influence of nanoclay additive on polymer morphology and structure and properties of resultant MB webs are discussed here.

EXPERIMENTAL

Meltblowing

Meltblown fabrics were produced from 1500 melt flow rate (MFR) PP with 0.5 wt % Closite Na⁺ with 1.25 and 2.5 wt % maleated PP compatibilizer. The 1500 MFR PP was provided by ExxonMobil Chemical Company, Baytown, TX. Natural nanoclay, Closite Na⁺ was obtained from Southern clay and then compounded with PP by Techmer PM, Clinton, TN. The master batch was mixed with PP to obtain the final concentration in the web and fed to the extruder. Webs were produced at two different air pressures 21 kN/m² (LP) and 41 kN/m² (HP). 15.4-cm wide research line with a single coat-hanger die manufactured by Accurate products at The University of Tennessee Nonwoven Research Laboratory, Knoxville, TN, was used. Processing conditions used are summarized in Table I. Die temperatures were in the range of 216 to 288°C. Webs were collected on a rotating collector drum at a die to collector distance of 38 cm, and resin throughput of 0.4 g/hole/min was used to achieve a targeted fabric weight of 25 grams per square meter (GSM). Different samples were produced and their respective compositions are included in Table II.

Testing and characterization

Meltblown samples were conditioned for 24 h in a conditioned laboratory before testing according to ASTM D1117-97 - Standard Test Method for Nonwoven fabrics.³⁶ Fiber diameters were measured using a polarized optical microscope. Thicknesses of fabric samples were measured using the TMI thickness tester as per the ASTM D5729-97. Tensile properties were determined using the United tensile tester. Tests were carried out using samples 25-mm wide and 75-mm gage length stretched to break at a uniform strain rate of 12.7 mm/min. Fabric stiffness

was estimated by measuring the bending length using the cantilever bending test method as per ASTM D5732-95. Bending length is the length of fabric at which, it bends under its own weight, which is taken as a means to account for nonwoven web stiffness. The rectangular fabric strip of 15×2.5 cm was selected in each case. Sample was placed on the horizontal platform with the engraved scale and slid at constant rate along the template. Length at which the sample bends under its own weight and makes an angle of 41.5° with the horizontal platform was measured. Each sample was tested four times on both sides (top and bottom) and by turning (right and left). Extent of color change in the meltblown web samples because of nanoclay additives was determined using a Miniscan XE hunter colorimeter.

Thermal analysis

Thermal analysis was carried out using the Mettler differential scanning calorimeter (DSC). Samples were heated from room temperature to 200°C at a heating rate of $10^\circ\text{C}/\text{min}$ in the N_2 atmosphere, held at that temperature for 10 min to ensure complete melting of all the crystals, and then cooled to room temperature at the rate of $65^\circ\text{C}/\text{min}$. Percentage of crystallinity, $X_c\%$, of nanoclay-incorporated samples were calculated from enthalpies of crystallization according to eq. (1).

$$X_c\% = \frac{\Delta H}{(1 - \phi)\Delta H_{100\%}} \times 100 \quad (1)$$

where ΔH is the measured heat of fusion of the sample, $\Delta H_{100\%}$ is the heat of fusion of the 100% crystalline PP, which is taken as 190 J/g for this study, and ϕ is the weight fraction of nanoclay additive.³⁷

The isothermal crystallization kinetics studies were also carried out using DSC. Samples were heated from room temperature to 200°C at a heating rate of $10^\circ\text{C}/\text{min}$ in the N_2 atmosphere and held at that temperature for 10 min to ensure complete melting of all the crystals. From molten state, samples were cooled to the crystallization temperature of 125°C at a rate of $-65^\circ\text{C}/\text{min}$. The relative crystallinity at different crystallization time, $X(t)$, was calculated from the ratio of the area of the exotherm up to time t divided by the total exotherm given by eq. (2). Where Q_t and Q_∞ are the heat generated at time t and infinite time, respectively, and dh/dt is the heat flow rate.²⁶

$$X(t) = \frac{Q_t}{Q_\infty} = \frac{\int_0^t \left(\frac{dh}{dt}\right) dt}{\int_0^\infty \left(\frac{dh}{dt}\right) dt} \quad (2)$$

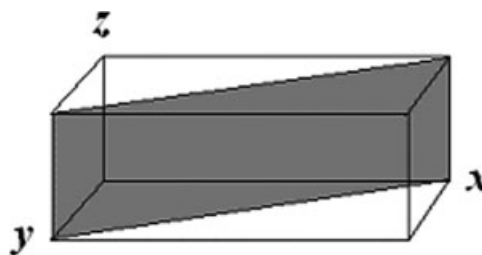


Figure 1 Representation of (110) plane of crystal.³⁸

Assuming that the relative crystallinity increases as a function of time, time-dependent relative crystallinity $X(t)$ by Avrami equation [eq. (3)] can be rearranged as eq. (4),

$$1 - X(t) = \exp(-Kt^n) \quad (3)$$

$$\log[-\ln(1 - X(t))] = \log K + n \log t \quad (4)$$

The value of n and K were calculated from slope and intercept of plot of $\log[-\ln(1 - X(t))]$ versus $\log(t)$. Where n is the Avrami exponent, which is nucleation and growth parameter, and K is the rate constant, which is nucleation-dependent term that describes the crystallization rate, and t is the crystallization time.^{21,22} From the relative crystallinity results, crystallization half time $t_{1/2}$ and t_{max} were determined.

Wide-angle x-ray diffraction

Wide-angle x-ray diffraction (WAXD) of fiber samples was carried out using a Phillips X Pert Pro x-ray diffraction system in continuous scan mode to evaluate crystallinity and crystal size. Equatorial scans were obtained from $2\theta = 2^\circ$ to 30° in steps of 0.01° and a dwell time of 4 s, operated at 45 kV and 40 mA. Crystal size (t) was calculated using the Scherrer Equation [eq. (5)],

$$t = \frac{0.9\lambda}{B \cos \theta_B} \quad (5)$$

where λ is wavelength in \AA and B is measured full-width half-maximum intensity of (110) reflection peaks. The crystal size (t) represents the dimension of rectangle passing through the (110) axis as shown in Figure 1.²⁸

Electron microscopy

To obtain the sections for transmission electron microscopy (TEM) analysis, fiber webs were embedded in epoxy block as shown in Figure 2. Sections of thickness $<70 \text{ nm}$ were cut from meltblown web composite using RMC Power tome CRX microtome equipped with diamond knife. Sections were stained

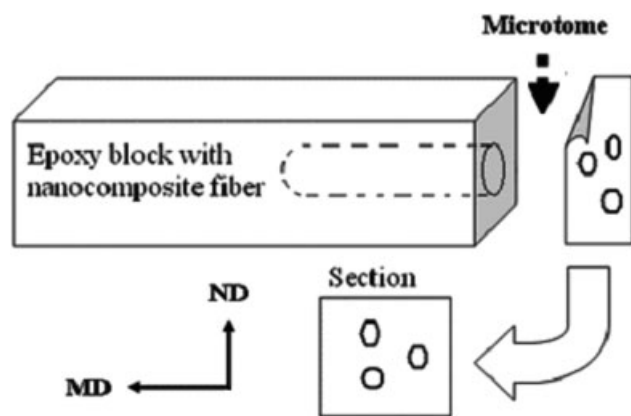


Figure 2 Schematic representation of TEM sample sectioning of fiber nanocomposites.

for 48 h using osmium tetroxide (OsO₄). TEM images of sections were obtained using a Hitachi H-800 electron microscope operated at 75 kV.

Scanning electron microscopic (SEM) photographs of the meltblown web surface and cross-sections were taken using the Leo 1215 Field emission gun. The samples were coated for 10 s using the SPI sputter coater. Image magnification was in the range of 100× to 1700×.

Oxford Pentafet energy dispersive x-ray spectroscopy (EDS) system was used in conjunction with SEM to evaluate the elemental composition of agglomerate in shots. ZAF Quantitative method: ZAF (3 iterations) with the system resolution of 127 eV and running Link ISIS software were used for EDS data analysis.

Optical microscopy was used to understand the crystallization, especially to observe spherulite growth under quiescent conditions. Control PP MB web sample and MB web samples with clay additive were kept in between glass plate and cover slide. Samples were isothermally melted at 205°C using hot press for 10 min. After 10 min, the hot press was switched off and allowed to cool on the heated plate of hot press. Average thickness of the crystallized film was <200 μm. Spherulite images were analyzed using Olympus BX51 polarized optical microscope.

TABLE III
Properties of Meltblown Web

Sample	Thickness (mm)	Air Permeability (g/m ²)	Bending Length (cm)	Yellowness (b)
Control MB	0.5	25	4	0.5
1LP	0.4	26	6	0.9
1HP	0.4	25	5	0.9
2LP	0.4	25	7	0.6
2HP	0.4	25	7	0.5

Nucleation density of spherulite N reported in the literature is given by eq. (6):

$$N = \left(\frac{3}{4}\pi\right)\left(\frac{D_m}{2}\right)^{-3} \quad (6)$$

where D_m is the maximum attainable diameter of spherulite before impingement.³⁹

RESULTS AND DISCUSSION

Some of the physical properties of the meltblown webs are summarized in Table III. Presence of nanoclay additives did not improve any of these properties in meltblown webs. Compared with control, air permeability of web with additives was 10 to 75% higher. Results of web bending length and air permeability prove the formation of stiffer webs with open web structure. Results of fiber diameter measured using optical microscope are shown in Figure 3. Average fiber diameter, coefficient of variation, and standard deviation were high for meltblown web samples with clay, especially the 1LP. This is expected because the presence of clay affects processing, and in turn, variability in MB. Web with open structure is the result of overall increase in fiber diameter. Tensile strength and elongation in machine direction (Fig. 4) were poor in the presence of additives. The sample 1LP (produced at low air pressure) showed low mechanical properties and higher variability in structure compared with rest of the samples. These changes in the properties of webs result from change in polymer microstructure because of well-dispersed clay additive.

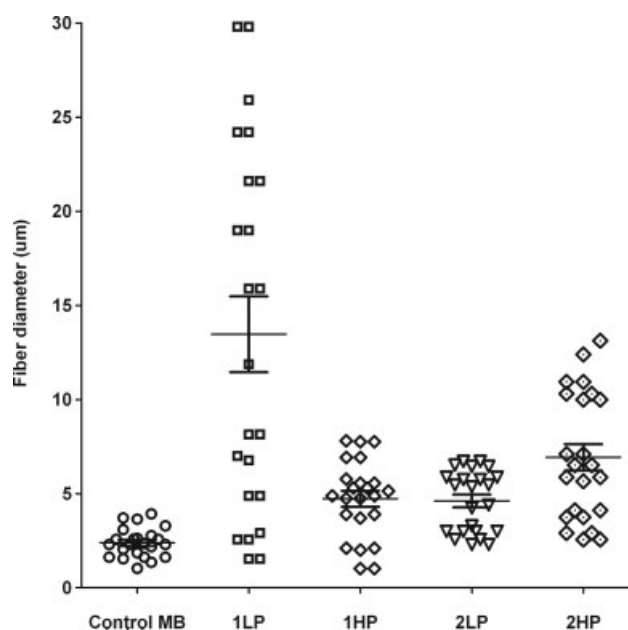


Figure 3 Meltblown web fiber diameter measurements.

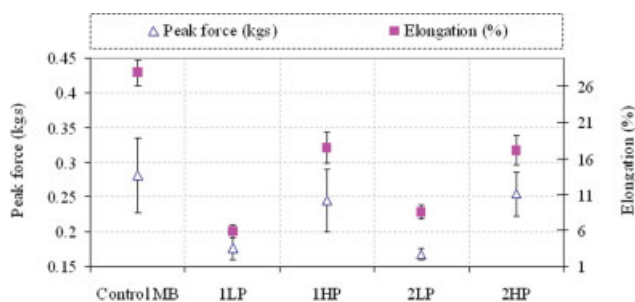


Figure 4 Tensile properties of web. [Color figure can be viewed in the online issue, which is available at www.interscience.wiley.com.]

The WAXD scans of different meltblown web samples are shown in Figure 5. The scans do not show any peaks corresponding to natural nanoclay that occurs around 2θ of 6.07° reconfirming good dispersion or delamination of the clay platelets beyond 100 \AA . The delaminated structure or loss of ordered structure is probably due to higher level of shear involved in the extruder.

Cooling of PP melt in the MB process is nonisothermal and hence produces mesophase of low order known as smectic state.⁴⁰ As evident from the WAXD scans, compared with control meltblown web, samples produced with clay additive have well-developed monoclinic crystalline peaks that are due to nucleating effect of nano additives. Results of crystallinity wt % and crystal size measured by WAXD are summarized in Figure 6. Results do not show any specific trend with most of the samples having similar values.

TEM micrographs of MB web samples with additives are shown in Figures 7–10. Micrographs reveal significant dispersion and delamination of clay platelets, which is due to the high MFR of PP resin and

also higher shear rate experienced by concentrates in extruder. Clay platelets in case of sample 1LP (Fig. 7) show complete dispersion of clay additives through fiber section. Small delaminated stacks and intercalated tactoids were observed in 1HP, 2LP, and 2HP (shown in Figs. 8–10). TEM micrographs also reveal loss of ordered clay platelet structure in all the fiber web samples that explain the reason for absence of peak corresponding to clay stacks in WAXD analysis.

The small agglomerates and intercalated stacks present during compounding might have been changed to delaminated structure because of high shear extrusion involved in MB processing. Additionally, lower molecular weight of the resin in MB will also make the intercalation easier. The delaminated structure is the reason for disappearance of peaks corresponding to nanoclay.

Thermal analysis results obtained from the DSC cooling scans are summarized in Table IV. Results do not show any specific trend. Crystallinity % of web with 2.5 wt % compatibilizer is slightly lower. Sample 1LP has higher crystallinity compared with rest of the fiber webs, which might be due to the very high exfoliated fiber morphology evident from the TEM micrographs.

Results of relative crystallinity $X(t)$ versus time for different web samples estimated from the isothermal crystallization kinetics are included in Figure 11. From the relative crystallinity results, it is evident that mechanism of crystallization is different for webs with nanoclay additives. Sigmoid shape is observed for all the samples except difference in saturation times. Sigmoid shape represents initial rate of phase change followed by subsequent slowing down as growing bodies impinge. Sample with additives attain saturation before control PP.

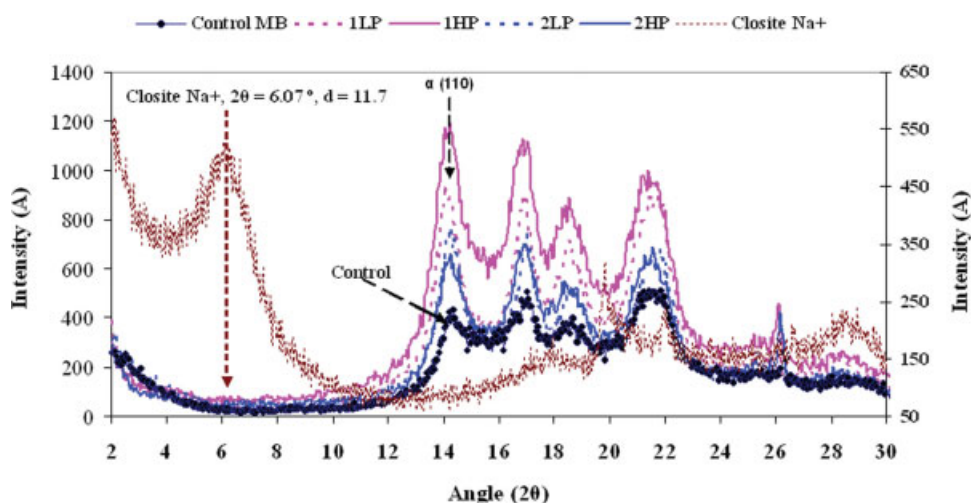


Figure 5 WAXD scans of meltblown web samples. [Color figure can be viewed in the online issue, which is available at www.interscience.wiley.com.]

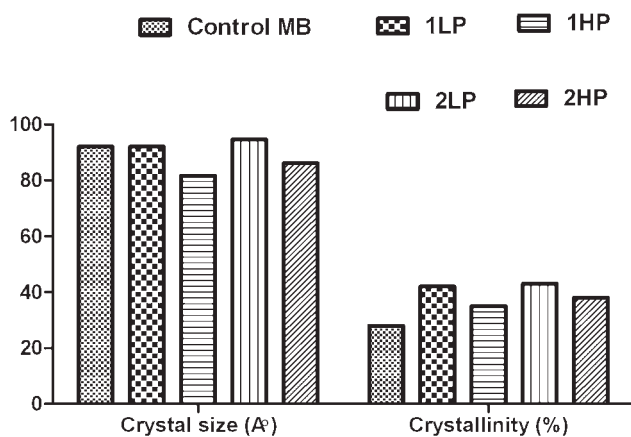


Figure 6 Results of fiber crystallinity (%) and crystal size (Å) of meltblown samples.

Results of isothermal crystallization parameters obtained from Avrami analysis are summarized in Table V. Avrami exponent n for nanocomposites and control PP varied from 1 to 2, which indicates spherulitic form of crystal growth. Sample 2HP has n of 1.4, which represents rod-like growth from instantaneous nuclei according to the literature.⁴¹ Also, fractional value of n indicates the presence of multiple growth morphologies and two different types of nucleation mechanisms.^{42,43} Total time for crystallization (t -max) for sample 1LP was 57% lesser compared with control PP. Overall, total time for crystallization (t -max) for samples with additives was 33–57% lesser when compared with control MB.

In the presence of the clay additive, the rate of crystallization, mechanism of heat transfer, cooling rate, and kinematics are different. Having additives facilitate the web to cool at faster rate compared with control PP web. Increased crystallization kinetics and higher cooling rate cause the individual fibers to solidify faster compared with neat resin, which minimizes the extent of interfacial bonding between the fibers. Hence, the elongation and strength of meltblown webs in the presence of additive are lower compared with that of the control.⁴⁴ These differences contribute to the difference in the observed web structure. Optimization of process conditions might help bring the property benefits.

Polarized light micrographs and number of spherulite in unit area for different PP samples are shown in Figure 12(a,d). The pronounced Maltese cross-extinction pattern is observed for neat PP as shown in Figure 12(a), whereas smeared four leaf-clove pattern is observed for samples 1 and 2 with 0.5% clay.³⁹ Kang et al.²⁰ observed heterogeneous nucleation mechanism and decrease in spherulite size from 155 μm in neat PP to 12 μm in the case of PP with 8 wt % clay additives.

Micrographs show well-developed spherulites size of $\approx 100 \mu\text{m}$ for control PP. The spherulites size of control PP is larger than that of concentrates with nanoclay additives. Average number of spherulites per area (volume fraction) of material studied is shown in Figure 12 (d). Results confirm nucleating effect of additives even at 0.5% add-on level. The coefficient of variation (CV) of number of spherulites in unit area observed is very high for sample with additives, which indicates variation of microstructure in sample [Fig. 12(d)]. Acceleration of crystallization and decrease in crystal size are due to the large number of spherulites per unit area.^{39,45–48}

The maximum attainable diameter (D_m) of spherulite and nucleation density (N) for different concentrates is included in Figure 13(a,b). The maximum attainable diameter further decreased for sample with nanoclay additives that indicate significant change in microstructure in the presence of additives. High nucleation density explains the differences in the relative crystallinity results. CV for the sample 1 is higher compared with control MB and sample 2, which might be due to the variation in dispersion of clay stacks obtained in TEM micrographs.

Slightly higher secondary crystallization time for sample with additives is due to the time involved in growth and to fill the interspaces between the spherulites.⁴⁹ The maximum spherulite diameter of

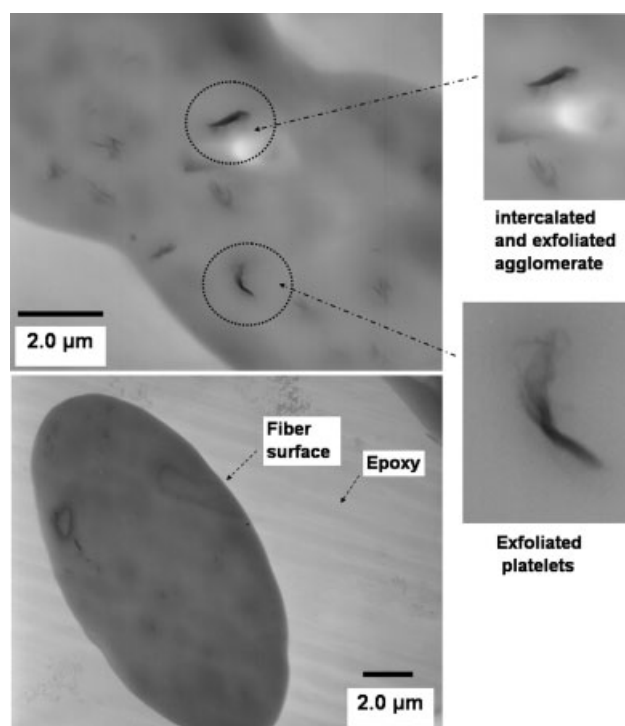


Figure 7 TEM image of MB web 1LP with 0.5 wt % nano clay.

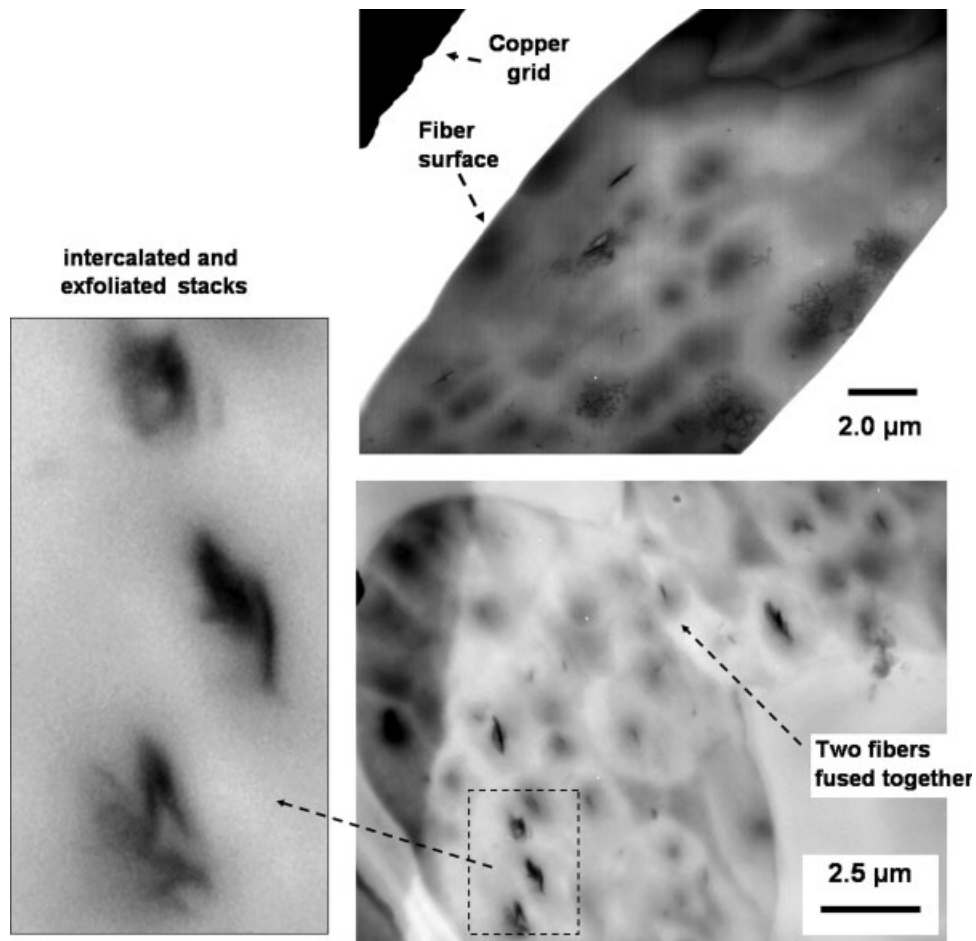


Figure 8 TEM image of 1HP MB web with 0.5 wt % nano clay.

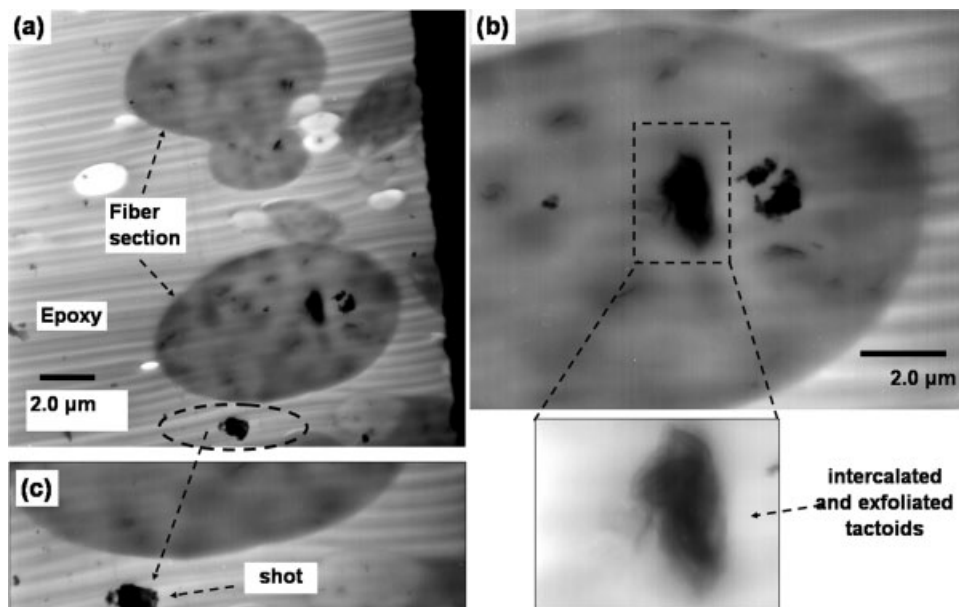


Figure 9 TEM micrograph of 2LP with 0.5 wt % nanoclay, (a) section with 3 fibers, (b) magnified image of fiber section with clay agglomerate, and (c) section of shot.

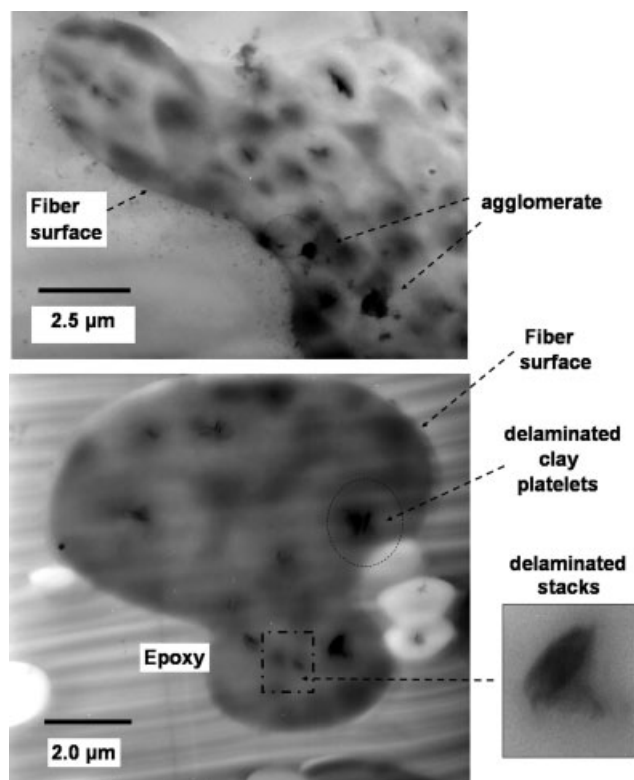


Figure 10 TEM micrograph of 2HP with 0.5 wt % nanoclay.

control PP observed in this study is $\approx 125 \mu\text{m}$, which is less than the spherulite diameters of PP reported in the literatures ($\approx 150\text{--}800 \mu\text{m}$),^{39,50} which is due to high MFR (1500 MFR) PP used in this study.

SEM micrographs of control and 1LP surface [Fig. 14(a–d)] clearly show increase in fiber diameter variation and shot formation for sample with clay. Figure 14(e) shows the SEM micrograph of section of shots found on the 1LP web sample. Some of these shots had clay agglomerates in them as reconfirmed by EDS elemental composition results. Fiber diameter shows much higher variability for webs with additives. In our previous studies, increase in shear viscosity has been observed for PP–clay concentrates.^{51,33} Increase in viscosity leads to increase in the fiber diameter variation.

Control resin formed better meltblown webs with fine fiber diameter and lower coefficient of variation.

TABLE IV
DSC Cooling Segment Results for MB Web

Sample	Control MB	1LP	1HP	2LP	2HP
Clay wt %	0	0.5	0.5	0.5	0.5
Onset (°C)	125	124	124	121	124
Peak (°C)	119	120	120	116	118
End set (°C)	115	113	114	111	110.4
integral (J/g)	737	840	825	725	803
normalized (mJ)	98	104	101	91	96
Crystallinity (%)	52	55	53	48	51

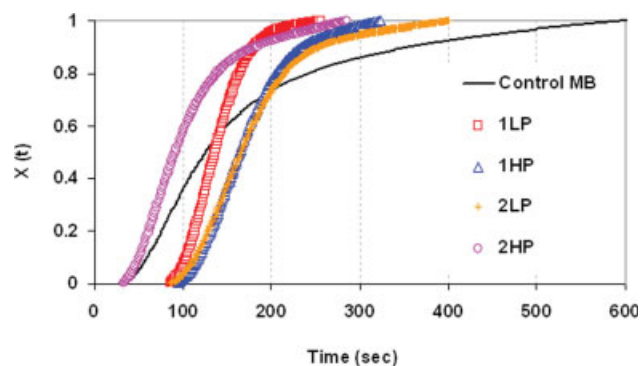


Figure 11 Relative crystallinity versus crystallization time of different MB web samples from DSC thermograms. [Color figure can be viewed in the online issue, which is available at www.interscience.wiley.com.]

Web produced at high air pressure had lower fiber diameter variation in the final web compared with that of webs produced at lower air pressure indicating formation of fine fibers with increase in primary air speed. Bresee³³ reported similar results of fiber diameter variation with different air pressure for neat PP resins.

In the meltblown process, fiber orientation and attenuation take place in semimolten state. Fibers remain hot even after lay down on collector and continue to crystallize on the collector. Some fibers fuse and form attenuated webs by contact in hot condition. Final web structure is developed after lay down in fused state on collector drum.

In this situation, increase in shot content is due to the increased melt viscosity in the presence of clays. Increased melt viscosity increases the fiber diameter and causes web variation. In earlier studies, it has been proved that fine fibers cool faster, orient, and stick together to form better meltblown webs. Fiber webs with increased fiber diameter and diameter variation cool at a slower rate. Irregularity and increase in cooling rate also result in the melt fusion and number of shots.^{51,33}

CONCLUSIONS

Influence of nanoclay additive and different percentage of compatibilizer on the structure, morphology, and mechanical properties of PP meltblown webs

TABLE V
Avrami Parameters for Different MB Web Samples

Sample	<i>n</i>	<i>K</i>	<i>t</i> _{1/2} (min)	<i>t</i> -max (min)	Hf (j/g)
Control PP	1.5	0.33	2	10	61
1LP	1.8	0.59	2	4	87
1HP	1.5	0.28	3	5	81
2LP	1.7	0.28	3	7	89
2HP	1.4	0.35	2	5	69

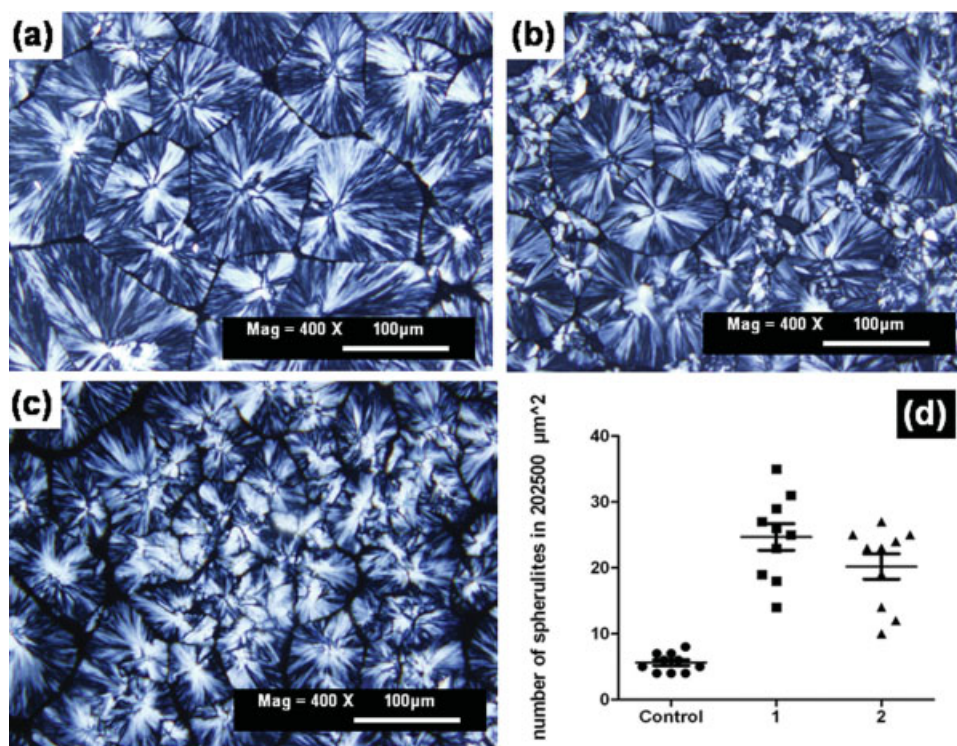


Figure 12 Polarized light micrographs of (a) control polypropylene, (b) sample 1 with 0.5 wt % nanoclay additive, (c) sample 2 with 0.5 wt % nanoclay additive, and (d) number of spherulite in unit area for different polypropylene samples. [Color figure can be viewed in the online issue, which is available at www.interscience.wiley.com.]

was studied. Samples were produced with 0.5% add-on level at two different air pressures. The peak corresponding to clay additives was not observed in WAXD scans for any sample with clay additive. TEM micrographs revealed significant dispersion of clay stacks but the ordered clay platelet structure was not observed in any of the produced MB web samples. Clay additive did not lead to any improvements in mechanical properties in the case of melt-blown webs. Compared with control MB, stiff, open, weak structure was obtained for samples with clay additives. Air permeability was about 10 to 75%

higher than that of control. MD strength dropped by about 9 to 35% compared to that of control MB web.

The property differences observed are the result of higher crystallization kinetics and resultant change in polymer microstructure in the presence of additives. Because of high nucleation density, crystallization time was about 30–57 % lower for webs with clay additive compared with that for control PP. With further process optimization, fiber diameter can be reduced and we might be able to get better properties. This study has shown that by using a suitable compounding method, nanoparticle reinforced fibers and

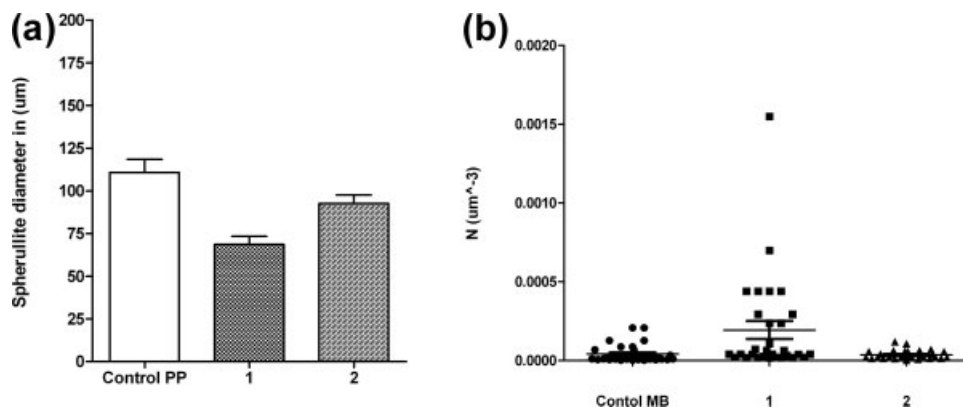


Figure 13 (a) Average maximum attainable diameter of spherulite in different polypropylene samples. (b) Nucleation density for different polypropylene samples.

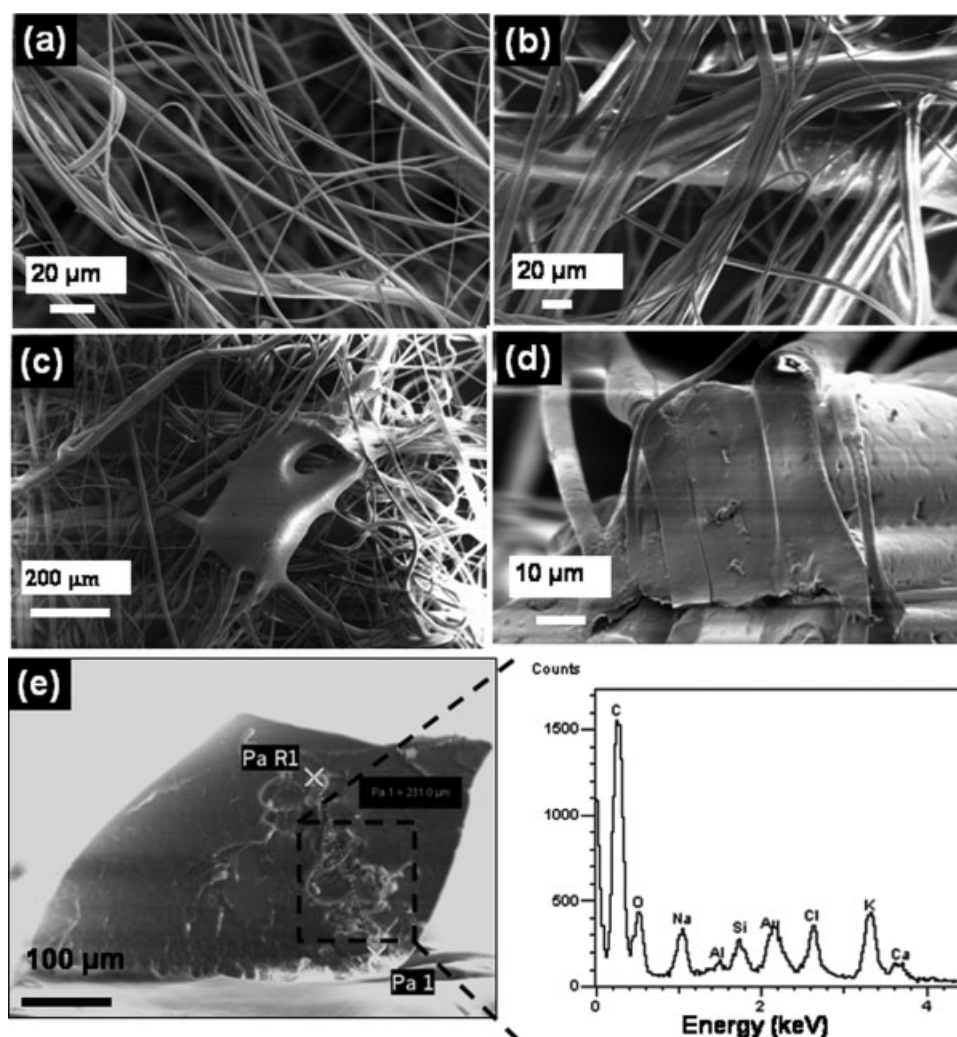


Figure 14 SEM micrograph of (a) control MB web, (b) web 1LP, (c) shots on 1LP, (d) cross-section of fiber web1LP, (e) SEM micrograph of cross-section of shots of 1LP web sample (nanoclay platelet clusters within agglomeration is reconfirmed).

fibrous products can be produced using conventional production machinery. Such an approach can be used to incorporate other nanoparticles as well.

The authors thank the staff of The University of Tennessee Nonwoven Research Laboratory for their help in sample preparation. Special thanks to Techmer PM, Clinton, TN, for providing the concentrates, and to ExxonMobil Chemical Company, Baytown, TX, for providing the PP resin.

References

- Bhat, G. S.; Zhang, Y.; Wadsworth, L. C. In *Processing of the Tappi Nonwoven Conference, 1992*, pp 61–68.
- Kotra, R.; Rong, H.; Dahiya, A.; Kamath, M. G.; Hegde, R. R.; Melt blown Technology. Available at: <http://web.utk.edu/~mse/Textiles/Melt%20Blown%20Technology.htm>. Accessed February 2009.
- Picard, E.; Vermogen, A.; Gérard, J. F.; Espuche, E. *J Membr Sci* 2007, 292, 133.
- Kojima, Y.; Usuki, A.; Kawasumi, M.; Okada, A.; Fukushima, Y.; Kurauchi, T.; Kamigaito, T. *J Mater Res* 1993, 85, 1185.
- Vaia, R. A.; Price, G.; Ruth, P. N.; Hieu, N. T.; Joseph, L. *Appl Clay Sci* 1999, 15, 67.
- Loo, L. S.; Gleason, K.; Karen, K. *Polymer* 2004, 45, 5933.
- Nanoclays. Available at: <http://www.nanoclay.com/main2.html>. Accessed February 2005.
- Kojima, Y.; Matsuoka, T.; Takahashi, K.; Kurauchi, T. *J Mater Sci Lett* 1993, 12, 1714.
- Lincoln, D. M.; Vaia, R. A.; Wang, Z. G.; Hsiao, B. S. *Polymer* 2001, 42, 1621.
- Brindly, S. W.; Brown, G. *Crystal Structure of Clay Minerals and Their X-Ray Diffraction*, London, 1980.
- Leroux, F.; Aranda, P.; Besse, J. P.; Hitzky, E. R. *Eur J Inorg Chem* 2003, 6, 1242.
- Greenland, D. J. *J Colloid Sci* 1963, 18, 647.
- Lu, X. F.; Hay, J. N. *Polymer* 2001, 42, 23.
- Krishnamoorti, R.; Giannelis, E. P. *Macromolecules* 1997, 30, 4097.
- Fornes, T. D.; Paul, D. R. *Polymer* 2003, 44, 3945.
- Liu, X.; Wu, Q. *Polymer* 2001, 42, 10013.
- Boykin, T. L.; Moore, R. B. *Polym Prepr (USA)* 1998, 39, 393.
- Jimenez, G.; Ogata, N.; Kawai, H.; Ogihara, T. *J Appl Polym Sci* 1997, 64, 2211.
- Yangchuan, Ke.; Long, C.; Qi, Z. *J Appl Polym Sci* 1999, 71, 1139.

20. Kang, X.; He, S. Q.; Zhu, C. S.; Wang, L. Y. *J Appl Polym Sci* 2004, 95, 756.
21. Avrami, M. J. *J Chem Phys* 1939, 7, 1103.
22. Avrami, M. J. *J Chem Phys* 1940, 8, 212.
23. Rodríguez, F. J. *Polym Eng Sci* 2007, 47, 1889.
24. Hegde, R. R.; Bhat, G. S. In *Influence of Nanoclay on Morphology of Polymer Films*, Fiber Society Conference, May, 2007.
25. Douwe, H.; Bart, G.; Igor, D.; Gabriel, G. *Polymer* 2006, 47, 1620.
26. Weng, W.; Chen, G.; Wu, D. *Polymer* 2003, 44, 8119.
27. Ergungor, Z.; Cakmak, M.; Batur, C. *Macromol Symp* 2002, 185, 259.
28. Zhang, X.; Yang, M.; Zhao, Y.; Zhang, S.; Dong, X.; Liu, X.; Wang, D.; Xu, D. *J Appl Polym Sci* 2004, 92, 552.
29. Xiao, W.; Yu, H.; Han, K.; Yu, M. *J Appl Polym Sci* 2005, 96, 2247.
30. Joshi, M.; Viswanathan, V. *J Appl Polym Sci* 2006, 102, 2164.
31. Toshniwal, L.; Fan, Q.; Ugbolue, S. C. *J Appl Polym Sci* 2007, 106, 706.
32. Mani, G.; Fan, Q.; Ugbolue, S. C.; Eiff, I. M. *AATCC Rev*, 2003, 3, 22.
33. Bresee, R. R. *J Eng Fibers Fabrics* 2006, 1, 1.
34. Bresee, R. R. *International Nonwovens Technical Conference*, 2006, p 513.
35. Bhat, G. S.; Hegde, R. R.; Kamath, M. G.; Deshpande, B. *J Eng Fibers Fabrics* 2008, 3, 3.
36. *Standard Test Methods for Nonwoven fabrics*. In *ASTM D1117-97*.
37. *METTLER TOLEDO DSC 822e STARe Software user manual DSC evaluations*.
38. Cullity, B. D.; Stock, S. R. *Elements of X-Ray Diffraction*, 3rd ed.; Prentice Hall: New Jersey, 2001, pp 556–557.
39. Maiti, P.; Nam, P. H.; Okamoto, M.; Hasegawa, N.; Usuki, A. *Macromolecules* 2002, 35, 2042.
40. Hendra, P. J. *Polymer* 1984, 25, 785.
41. Sharples, A. *Introduction to Polymer Crystallization*; St Martin's Press: New York, 1966.
42. Wanderlich, B. *Macromolecular Physics*; Academic Press Inc: New York, 1976, Vol. 2.
43. Fukada, A. *Crystallization Kinetics and Annealing Behavior of Thermotropic Liquid Crystalline Polymer*; The University of Tennessee: Tennessee, 1991.
44. Amish, L. M. *Benefits of Inorganic Additives in Meltblown Polypropylene*; INTC: Texas, 2008.
45. Hambir, S.; Bulakhm, N.; Jog, J. P. *Polym Eng Sci* 2002, 42, 1800.
46. Svoboda, P.; Zeng, C.; Wang, H.; James, L.; David, L.; Tomasko, L. *J Appl Polym Sci* 2002, 85, 1562.
47. Ma, J.; Zhang, S.; Qi, Z.; Li, G.; Hu, Y. *J Appl Polym Sci* 2002, 83, 1978.
48. Pozsgay, A.; Frater, T.; Papp, L.; Sajo, I.; Pukanszky, B. *J Macromol Sci Part B Phys* 2002, 41, 1249.
49. Albano, C.; Papa, J.; Ichazo, M.; González, J.; Ustariz, C. *Compos Struct* 2003, 62, 291.
50. Nowacki, R.; Monasse, B.; Piorkowska, E.; Galeski, A.; Haudin, J. M. *Polymer* 2004, 45, 4877.
51. Bresee, R. R.; Ko, W. C. *Int Nonwovens J* 2003, 12, 21.
52. *DSC 822e Thermal analysis user manual*. In *METTLER TOLEDO*.